Imaging Neuroscience
an open access journal

Research Article

Brain connectivity correlates of breathing and cardiac patterns in epilepsy: A study including SUDEP cases

Michalis Kassinopoulos[a,b], Nicolo Rolandi[a,b], Laren Alphan[a], Ronald M. Harper[c,d], Joana Oliveira[a,e], Catherine Scott[a,e], Lajos R. Kozák[a,f], Maxime Guye[g,h], Louis Lemieux[a,b,*], Beate Diehl[a,b,e,*]

[a]UCL Queen Square Institute of Neurology, University College London, London, United Kingdom
[b]Epilepsy Society, Chalfont St. Peter, Buckinghamshire, United Kingdom
[c]UCLA Brain Research Institute, Los Angeles, CA, United States
[d]Department of Neurobiology, David Geffen School of Medicine at UCLA, Los Angeles, CA, United States
[e]Department of Clinical Neurophysiology, National Hospital for Neurology and Neurosurgery, UCLH, London, United Kingdom
[f]Department of Neuroradiology, Medical Imaging Centre, Semmelweis University, Budapest, Hungary
[g]Aix Marseille Univ, CNRS, CRMBM UMR 7339, Marseille, France
[h]APHM, Hôpital de la Timone, CEMEREM, Marseille, France

*These authors contributed equally to this work

Corresponding author: Michalis Kassinopoulos (m.kassinopoulos@ucl.ac.uk)

ABSTRACT

Sudden unexpected death in epilepsy (SUDEP) is the leading cause of premature mortality among people with epilepsy. Evidence from witnessed and monitored SUDEP cases indicates seizure-induced cardiovascular and respiratory failures; yet, the underlying mechanisms remain obscure. SUDEP occurs often during the night and early morning hours, suggesting that sleep or circadian rhythm-induced changes in physiology contribute to the fatal event. Resting-state functional MRI (fMRI) studies have found altered functional connectivity between brain structures involved in cardiorespiratory regulation in later SUDEP cases and in individuals at high risk of SUDEP. However, those connectivity findings have not been related to changes in cardiovascular or respiratory patterns. Here, we compared fMRI patterns of brain connectivity associated with regular and irregular cardiorespiratory rhythms in SUDEP cases with those of living epilepsy patients of varying SUDEP risk and healthy controls. We analysed resting-state fMRI data from 98 patients with epilepsy (9 who subsequently succumbed to SUDEP, 43 categorized as low SUDEP risk (no tonic–clonic seizures (TCS) in the year preceding the fMRI scan), and 46 as high SUDEP risk (>3 TCS in the year preceding the scan)), and 25 healthy controls. The global signal amplitude (GSA), defined as the moving standard deviation of the fMRI global signal, was used to identify periods with regular ("low state") and irregular ("high state") cardiorespiratory rhythms. Correlation maps were derived from seeds in 12 regions with a key role in autonomic or respiratory regulation for the low and high states. Following principal component analysis, component weights were compared between the groups. We found widespread alterations in connectivity of precuneus/posterior cingulate cortex in epilepsy compared with controls in the low state (regular cardiorespiratory activity). In the low state, and to a lesser degree in the high state, reduced anterior insula connectivity (mainly with anterior and posterior cingulate cortex) in epilepsy appeared, relative to healthy controls. For SUDEP cases, the insula connectivity differences were inversely related to the interval between the fMRI scan and death. The findings suggest that anterior insula connectivity measures may provide a biomarker of SUDEP risk. The neural correlates of autonomic brain structural activity associated with different cardiorespiratory rhythms may shed light on the mechanisms underlying the fatal event in SUDEP.

Keywords: state-dependent functional connectivity, sympathovagal balance, SUDEP, anterior insula, breathing disturbances, cardiac arrhythmia

Received: 5 September 2024 Revision: 28 July 2025 Accepted: 9 September 2025 Available Online: 22 September 2025

1. INTRODUCTION

Sudden unexpected death in epilepsy (SUDEP) is the leading cause of premature death in patients with intractable epilepsy, with an annual incidence estimated at approximately 1.2 per 1,000 persons with epilepsy (Keller et al., 2018; Sveinsson et al., 2017; Thurman et al., 2017). SUDEP is defined as "the sudden, unexpected, witnessed or unwitnessed, nontraumatic, and nondrowning death in patients with epilepsy, with or without evidence for a seizure and excluding documented status epilepticus, in which postmortem examination does not reveal a structural or toxicologic cause for death" (Nashef et al., 2012). SUDEP imposes a substantial public health burden (Thurman et al., 2017) and, among neurological disorders, ranks second only to stroke in terms of potential years of life lost (Thurman et al., 2014). Frequent generalized and focal-to-bilateral tonic–clonic seizures (TCS; Fisher et al., 2017) are the greatest risk factors. Sleep and nocturnal TCS appear to facilitate SUDEP (Ali et al., 2017; Ryvlin et al., 2013). The pathophysiology of SUDEP remains poorly understood (Devinsky et al., 2016; Sveinsson et al., 2020), and seizure control is considered the most effective strategy for reducing risk of fatal outcomes. However, currently, strategies for assessing SUDEP risk on an individual basis are still lacking.

Epilepsy monitoring unit data from the MORTEMUS study (MORTality in Epilepsy Monitoring Unit Study) suggest that SUDEP results from cardiorespiratory dysfunction induced by TCS (Ryvlin et al., 2013). Vilella et al. (2019) found that post-ictal central apnea occurs in one out of five TCS and was present in near-SUDEP and SUDEP cases, suggesting that breathing cessation may represent an important SUDEP biomarker. Cardiovascular parameters may also provide markers; heart rate and its variability, measured in the peri-ictal period (e.g., post-ictal mean heart rate; Arbune et al., 2020), are associated with markers of seizure severity that have been linked to SUDEP, such as the presence of TCS and duration of post-ictal generalized EEG suppression (PGES). However, although some patients succumb to SUDEP after a few seizures, others survive hundreds of similar attacks, which suggests the presence of additional pathophysiological mechanisms in SUDEP victims (Devinsky & Sisodiya, 2020). Reduced interictal heart rate variability (HRV) measured during wakefulness has also been associated with SUDEP (DeGiorgio et al., 2010; Sivathamboo et al., 2021), raising the possibility of chronic impairment in autonomic regulation in SUDEP. Further evidence of the role of chronic dysregulation is provided by the recent observation of abnormal heart rate responses during and after hyperventilation in patients who subsequently died of SUDEP (Szurhaj et al., 2021), and of volume changes in brain regions with key roles in autonomic regulation (Allen, Vos, et al., 2019; Mueller et al., 2018).

Functional MRI (fMRI) is a non-invasive neuroimaging tool that can evaluate functional connectivity (FC) between brain structures at a whole-brain level. Early fMRI studies focusing on FC revealed altered connectivity of regions involved in cardiorespiratory regulation such as the anterior cingulate cortex, thalamus, and regions of the brainstem in SUDEP cases and patients at high risk of SUDEP (Allen et al., 2017; Allen, Harper, et al., 2019; Tang et al., 2014). These studies, however, did not take into consideration the time-varying nature of FC observed on the scale of seconds to minutes, which may provide a more holistic understanding of brain functional organization (Chang & Glover, 2010; Preti et al., 2017). There is accumulating evidence that FC dynamics change with different autonomic and sleep states (Chang et al., 2013; Haimovici et al., 2017). Thus, examining the changes in FC occurring in different dynamic patterns of breathing or cardiovascular action, such as those that appear during different sleep states or other provocations, may reveal new insights into mechanisms that contribute to SUDEP different from those FC values obtained in stable physiological conditions.

In addition to the apparent role of sleep and nocturnal TCS, more attention to the state-dependent nature of autonomic manifestations is warranted. A stronger association exists between SUDEP and post-ictal rather than ictal central apnea (Vilella et al., 2019); whereas abnormally low HRV occurred in SUDEP during wakefulness, but not during sleep (Sivathamboo et al., 2021). Thus, examination of the state-dependent nature of autonomic influences on resting-state fMRI appears warranted. In particular, the observation that subjects who exhibit strong fluctuations in heart rate and breathing patterns during fMRI scans also show elevated global signal amplitudes (GSA), which reflect strong BOLD fMRI fluctuations globally in the brain (Orban et al., 2020; Power et al., 2017; Xifra-Porxas et al., 2021), and may be key to better understand SUDEP physiology.

We sought to characterize the patterns of FC in patients who eventually succumbed to SUDEP, living patients of varying SUDEP risk levels, and healthy controls, with respect to variations in regularity of cardiorespiratory rhythms. First, we used a publicly available fMRI dataset (Van Essen et al., 2013) with concurrent physiological recordings to demonstrate that the association of GSA with cardiac and breathing rhythms is maintained even within short fMRI scans (~15 minutes), with periods of high GSA corresponding to times with irregularities in cardiac or breathing activity, such as periods with transient apnea. Second, we characterized patterns of FC in SUDEP cases and epilepsy patients alive at the

time of this analysis by employing a state-dependent framework and GSA as a marker of cardiorespiratory variability. Moreover, given the well-documented success of FC measures in predicting symptom severity in individuals for a range of disorders (Du et al., 2017; Uddin et al., 2013; Yoo et al., 2018), we also investigated whether FC measures in SUDEP cases were associated with the time between the fMRI scan and SUDEP occurrence.

2. MATERIALS AND METHODS

The principal aim was to study the link between brain connectivity and autonomic activity in patients with epilepsy using a large resting-state fMRI dataset that did not comprise physiological recordings. This study consisted of two experiments: In Experiment 1, we employed a set of resting-state fMRI data that included concurrent recordings from a photoplethysmograph (PPG) and a respiratory belt to demonstrate that global signal amplitude (GSA) fluctuations reflect changes in cardiorespiratory activity. Previous studies defined GSA as the standard deviation of the global signal across the entire scan (Wong et al., 2013, 2016) and showed that GSA is linked to physiological parameters (Orban et al., 2020). Here, we computed GSA over significantly shorter durations, using a sliding window approach, to illustrate that the relationship of GSA with physiological parameters also is maintained at shorter timescales. Experiment 2 consisted of the characterization of the patterns of FC in patients with epilepsy using GSA as a marker for breathing and cardiac irregularities.

A methodological difference between the two datasets used in this study is the repetition time (TR): 0.72 seconds in the HCP data and 3 seconds in our own dataset. While faster TRs are generally advantageous for capturing high-frequency physiological signals, the physiological variables of interest in our study (heart rate, breathing rate, respiration volume, and PPG amplitude) fluctuate at lower frequencies (~0.1 Hz), which are well within the range captured by our sampling rate (0.33 Hz), satisfying the Nyquist criterion. Furthermore, previous work has shown that fMRI fluctuations related to these physiological variables can be reliably characterized even with slower TRs (Kassinopoulos & Mitsis, 2019, 2021). Therefore, we believe the TR difference does not significantly impact the validity of our findings.

2.1. Experiment 1: Association of fMRI global signal amplitude with variations in cardiorespiratory rhythms (HCP data)

To demonstrate that the global signal amplitude is linked to cardiorespiratory activity, we examined resting-state fMRI data from the Human Connectome Project (HCP; Van Essen et al., 2013) that included concurrent recordings from a photoplethysmograph (PPG) and a respiratory belt. A description of the preprocessing pipeline for the HCP dataset can be found in the Supplementary Material. Data from a subset of 400 healthy young participants previously characterized by good-quality physiological recordings through visual inspection in earlier studies (Kassinopoulos & Mitsis, 2019, 2022; Xifra-Porxas et al., 2021) were included. The global signal, defined as the mean fMRI time series averaged across all voxels in the grey matter, was computed from the fMRI data after volume realignment and high-pass filtering (0.008 Hz). Subsequently, the global signal amplitude (GSA), defined as the standard deviation of the global signal, was computed in a sliding window manner for window lengths ranging from 10 to 120 seconds (or equivalently, 14 to 167 time points) using the Matlab function *movstd*. A one-sample shift was applied between consecutive windows, and the standard deviation computed within a window was assigned to the center of the window in terms of time. In addition, the following four variables were obtained from the physiological recordings: (1) breathing rate; (2) respiration volume, as defined in Chang et al. (2009; i.e., moving standard deviation of respiratory signal with a window length of 6 seconds); (3) heart rate; and (4) PPG amplitude, defined as the amplitude of the oscillatory signal in the PPG (Kassinopoulos & Mitsis, 2021). Subsequently, the moving standard deviation of the physiological variables was also estimated for window lengths ranging from 10 to 120 seconds in 10-second increments. Then, for each window length, the correlation of the GSA with each of the four physiological variables was computed and averaged across all individuals, to determine the length that maximized the correlation without sacrificing temporal resolution.

2.2. Experiment 2: Characterization of the GSA-related patterns of FC in patients with epilepsy

2.2.1. Subjects

We retrospectively ascertained cases of SUDEP and high- and low-risk patients from the University College London Hospitals (UCLH) clinical database who had undergone an EEG-fMRI scan in the period between 2005 and 2015 (Coan et al., 2016). The inclusion criteria were (1) the availability of a resting-state EEG-fMRI scan and (2) a high-resolution T_1-weighted scan. The exclusion criteria were (1) large brain lesion or previous neurosurgery (we considered "large" as lesions extending across multiple lobes, involving deep brain structures, or causing significant mass effect—for example, tumors, vascu-

lar malformations—and typically larger than a small area of focal cortical dysplasia (FCD) or hippocampal sclerosis; (2) incomplete clinical or imaging data (e.g., abandoned scans); and (3) having died in the following years with a cause of death not related to SUDEP. Only patients alive at the time of writing were considered as low-risk or high-risk epilepsy controls.

Out of a cohort of 189 patients who underwent resting-state EEG-fMRI, 14 deaths were identified in the UCLH clinical database, of which 10 were classified as SUDEP based on their death certificate. One SUDEP case was excluded due to the presence of a large brain lesion. The remaining nine SUDEP cases (five females, mean age 26.2 ± 6.2 years) were classified as either probable or definite SUDEP based on the definitions proposed in Nashef et al. (2012). The 9 examined SUDEP cases were matched with 43 low-risk, 46 high-risk patients, and 25 healthy controls based on sex and age at the time of scan. High-risk patients were considered those who experienced more than three TCS in the year preceding the scan and low-risk patients were considered those who did not experience TCS. Only patients whose clinical records allowed for a clear classification into low- or high-risk groups based on tonic–clonic seizure frequency were included. This approach helped to maintain relatively balanced and homogeneous group sizes, avoiding the inclusion of cases with ambiguous risk profiles or incomplete data. Group demographics and clinical details are shown in Supplementary Table S1. The study was approved by our local research ethics committee, and all patients gave written informed consent.

2.2.2. Simultaneous EEG-fMRI acquisition

Scanning was performed at the Epilepsy Society (Chalfont St Peter, Buckinghamshire, UK) on a 3.0 Tesla GE (Signa excite HDX) scanner. A 20-minute (400 vol) T_2*-weighted fMRI scan was collected from each subject except for two patients who were scanned for 10 minutes. The fMRI scan was collected using a gradient-echo echo-planar-imaging with the following characteristics: repetition time (TR) = 3,000 ms, echo time (TE) = 30 ms, flip angle = 90°, matrix size = 64 x 64, field of view (FOV) = 24 x 24 cm^2, slice thickness = 2.4 mm with 0.6 mm gap, 44 slices, and voxel size = 3.75 x 3.75 x 3 mm^3. Subjects were instructed to keep their eyes closed, avoid falling asleep, and not think about anything in particular. A T_1-weighted image was also acquired using a FSPGR (fast spoiled gradient recalled echo) sequence, with the following parameters: matrix size = 256 x 256, FOV = 24 x 24 cm^2, slice thickness = 1.5 mm, 150 slices, and voxel size = 0.94 x 0.94 x 1.5 mm^3.

Scalp EEG signals and an electrocardiogram (ECG) signal were simultaneously acquired during fMRI scanning at 5 kHz using a 64-channel MR-compatible EEG system with a cap comprising ring Ag/AgCl electrodes (BrainAmp MR+; Brain Products GmbH, Gilching, Germany). The electrodes were placed according to the 10/20 system and referenced to electrode FCz.

2.2.3. Preprocessing of fMRI data

The preprocessing of fMRI data was conducted using the Statistical Parametric Mapping software (SPM12, Wellcome Trust Centre for Neuroimaging, London, UK, http://www.fil.ion.ucl.ac.uk/spm; Friston et al., 2007) in a Matlab environment (R2020a; Mathworks, Natick, Massachusetts, USA). The first five functional volumes were discarded to allow steady-state magnetization to be established, and the remaining volumes were realigned to correct for head movements. The structural image of each subject was co-registered to the mean realigned functional volume and, subsequently, underwent tissue segmentation into grey matter, white matter, and cerebrospinal fluid tissue compartments. The functional images, as well as the coregistered structural images and tissue compartment masks, were spatially normalized to the Montreal Neurological Institute (MNI) reference space using non-linear transformation.

To account for anatomical variability across participants and reduce thermal noise, all individual functional volumes were smoothed using a 5 mm full-width half-maximum (FWHM) Gaussian kernel. The fMRI time series were high-pass filtered at 0.008 Hz to avoid spurious correlations that arise from low-frequency fluctuations (Leonardi & Van De Ville, 2015).

We used the frame-wise displacement (FD) introduced by Salek-Haddadi et al. (2006), implemented here as calculated in Power et al. (2012), to identify and exclude subjects with high levels of motion, as motion can lead to systematic biases in FC studies (Kassinopoulos & Mitsis, 2022; Power et al., 2015; Savva et al., 2020; Xifra-Porxas et al., 2021). FD was calculated from the six motion realignment parameters, reflecting the extent of scan-to-scan head motion at each time point. Subjects who were characterized by mean FD larger than 0.25 mm were excluded. For the datasets included in this study, time points with FD larger than 0.2 mm were considered outliers, and corrected by linear interpolation.

Finally, to further mitigate the effects of motion and reduce contributions from physiological processes and scanner artefacts, we regressed the following nuisance effects from all voxel time series: the first 10 principal components extracted from all white matter voxel time series (Behzadi et al., 2007), 6 regressors related to

cardiac pulsatility artefacts obtained with the convolution model proposed in Kassinopoulos and Mitsis (2021) in conjunction with the R-wave peaks detected in the ECG (Supplementary Material—Section b), and the mean fMRI time series averaged across all voxels within the grey matter (Macey et al., 2004). The mean grey matter signal was considered a nuisance regressor—a practice known as global signal regression (GSR)—as there is accumulating evidence that the mean grey matter signal (also referred to as the global signal) reflects changes in heart rate and breathing patterns (Kassinopoulos & Mitsis, 2019; Xifra-Porxas et al., 2021). Note that although GSA, which is used in this study to probe regularities in cardiorespiratory activity, is derived from the grey matter signal, the two aforementioned signals are weakly correlated, with a group average correlation of -0.05 (±0.25) (for a GSA estimation with a sliding window length of 80 seconds).

2.2.4. Seed-based connectivity and spatial distribution pattern analysis

A seed-based FC analysis was employed with seeds consisting of regions with a key role in autonomic and respiratory regulation (Benarroch, 1993; Critchley et al., 2003; Lacuey et al., 2018; Song et al., 2018; Valenza et al., 2019). Specifically, the seeds consisted of the mean time series of voxels within the following 12 regions: anterior cingulate cortex, anterior insula, posterior insula, thalamus, amygdala, hippocampus, parahippocampal gyrus, precuneus/posterior cingulate cortex (PCu/PCC), cuneus, caudate, putamen, and Brodmann area 25. Those regions were defined based on parcels (i.e., non-overlapping contiguous regions) from the Brainnetome atlas (Fan et al., 2016).

As in Experiment 1, the global signal used to derive GSA was computed as the mean time series averaged across all voxels in the grey matter, after volume realignment and high-pass filtering (0.008 Hz), and before regressing out nuisance regressors. A window length of 80 seconds was used to derive the GSA, as this length was found in Experiment 1 to yield a strong association between the GSA and the physiological variables, while also preserving an adequate temporal resolution (see Results, Section 3.1). To identify periods of relatively stable versus unstable cardiorespiratory activity, we used GSA as a proxy. Specifically, we divided the GSA time series into quartiles and selected the time points in the lowest 25% (first quartile) to represent the "low state"—periods of more regular physiological rhythms—and the highest 25% (fourth quartile) to represent the "high state"—periods of more irregular rhythms. This classification is supported by results from Experiment 1 (see Fig. 2; Supplementary Fig. S2), which demonstrate that low GSA values correspond to periods of stable breathing and heart rate, while high GSA values coincide with transient apnea, heart rate surges, or fluctuations in PPG amplitude. These selected time points were then used to compute functional connectivity separately for each state (Fig. 1A). Time points that corresponded to the second and third quartile were discarded from the analysis.

The fMRI time series derived for each seed was correlated with all regions in the grey matter on a voxel-wise basis (Pearson correlation), considering the low and high states, separately. Time points that corresponded to the low state were concatenated before computing the Pearson correlation between seed and voxel time series. Likewise, time points in the high state were concatenated before computing the Pearson correlation. Importantly, while this process involves concatenating non-contiguous time points corresponding to each physiological state, the use of Pearson correlation as the metric of connectivity is inherently blind to the temporal order of the input data. That is, Pearson correlation evaluates the linear relationship between two signals regardless of the order of the observations. A similar strategy has been used in prior studies, such as Rai et al. (2024), where high-motion volumes were censored and the remaining parcel time series were concatenated across runs and days before computing the functional connectivity matrices.

The correlation values were then converted into z-scores using Fisher's transform (Fig. 1B). For each seed, the correlation maps were vectorized and concatenated across subjects and states, resulting in a two-dimensional matrix where rows represent subjects and states (e.g., a row may correspond to subject *i* in the low state), and columns correspond to voxels. Finally, the resulting matrix was decomposed through principal component analysis (PCA) to generate a set of FC patterns, also known as eigenconnectivities (Leonardi et al., 2013), and a set of weights reflecting the degree to which a subject expresses each of the FC patterns in a given state (Fig. 1C). To reduce the number of tests, the subsequent analysis was restricted to the components explaining the highest fraction of variance with a 90% of cumulative variance.

2.2.5. Permutation-based statistical analysis

The PCA weights obtained for each component were compared between the four groups (SUDEP, high-risk patients, low-risk patients, controls) using ANOVA, considering the weights associated with the low and high states separately. The *F*-statistics associated with pairs

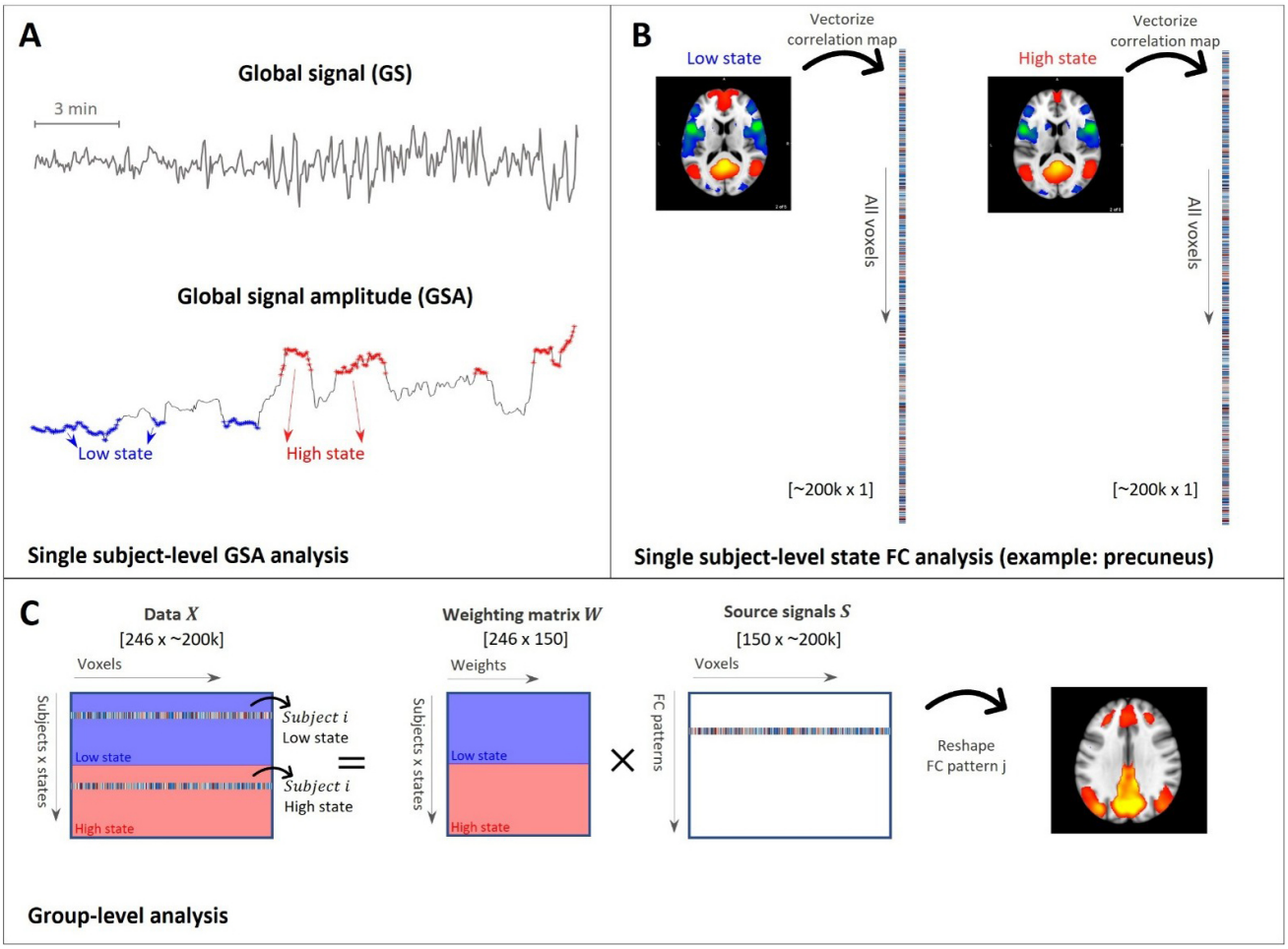

Fig. 1. Experiment 2. Analytical framework for characterizing functional connectivity (FC) in individuals based on a linear combination of group-level FC patterns. (A) The global signal amplitude (GSA), defined as the moving standard deviation of the fMRI global signal (window length: 80 seconds), was computed and used to determine times with regular ("low state") and irregular ("high state") cardiorespiratory activity. (B) Subsequently, for each subject, state, and seed region of interest (here, precuneus/posterior cingulate cortex), we computed whole-brain correlation maps represented in vectorized form. (C) Finally, for each seed, the connectivity strength vectors were concatenated across subjects and states, and the resulting two-dimensional matrix (left of the equal sign) was fed into a principal component analysis (PCA) to derive the underlying group-level FC patterns.

of components and states were mapped to *p*-values based on a null distribution generated using permutation tests. To generate the null distribution of *F*-statistics, 10,000 permutations were performed where in each permutation the subjects were randomly assigned to one of the four groups keeping the size of each group same to the size of the real groups. Subsequently, the *F*-statistics obtained from all examined components (i.e., the M most significant components that corresponded to a 90% cumulative variance), the 12 seeds, and the 2 states were pooled to generate the null distribution. The alpha level was set at $p < 0.05$ which was corrected for multiple comparisons (M = 150, 12 seeds, 2 states) using Bonferroni correction. For the components found to discriminate between the four groups, we explored the possibility that the involvement of a component in brain connectivity is associated with the time interval between the fMRI scan and occurrence of SUDEP using the Pearson's correlation coefficient.

2.2.6. *Large-scale network involvement*

Finally, we estimated the level of involvement of the seven large-scale networks reported by Yeo et al. (2011) for each connectivity component found to discriminate between the four groups. This was done by calculating each component's spatial overlap (Sørensen–Dice coefficient) with Yeo's large-scale networks using the *ICN_Atlas* toolbox (Kozák et al., 2017). The sign of the connectivity component was taken as that of its Sørensen–Dice coefficient.

3. RESULTS

3.1. Experiment 1: Association of fMRI global signal amplitude with variations in cardiorespiratory rhythms (HCP data)

The GSA was strongly correlated with the standard deviation of each of the four examined physiological variables (breathing rate, respiration volume, heart rate, and PPG amplitude; Supplementary Fig. S1) in the HCP data (Van Essen et al., 2013). The strongest association was observed for respiration volume; furthermore, increasing the window length from 20 to 80 seconds led to a significant increase of the correlation from 0.29 (±0.02) to 0.53 (±0.03) which remained at similar levels for longer lengths. A window length of approximately 80 seconds increased the correlation of GSA with breathing rate (0.34 ± 0.03) and PPG amplitude (0.30 ± 0.03). Figure 2 shows the breathing-related and fMRI signals for a subject where the levels of GSA co-fluctuate with variations in respiration volume. For instance, we observed that periods with strong fluctuations in respiration volume (e.g., 200–500 seconds) were characterized by higher levels of GSA, as compared with periods with regular breathing activity (e.g., 500–600 seconds). Finally, while a similar association of GSA with respiration volume was observed, for several subjects, high levels of GSA often corresponded to periods with transient apnea (i.e., brief pauses of breathing activity; Supplementary Fig. S2A), transient increase in heart rate (Supplementary Fig. S2B), or variations in PPG amplitude (Supplementary Fig. S2C). Therefore, GSA is strongly driven by variations in cardiovascular and breathing activity, although it cannot distinguish the former from the latter.

3.2. Experiment 2: Characterization of the GSA-related patterns of FC in patients with epilepsy

Three low-risk and one high-risk epilepsy patients were excluded due to excessive motion (mean FD > 0.25 mm) resulting in a cohort of 119 subjects (57 women; mean age 30.4 ± 8.4): healthy controls, 25; low-risk, 40; high-risk, 45; SUDEP, 9. The sex and age distributions were similar between the four groups (Supplementary Table S1). In addition, the four groups exhibited similar levels of fMRI scan-wise motion as assessed with ANOVA ($F = 1.3$; $p > 0.05$).

3.2.1. Identification of autonomic structures with significant group differences

The seed-based correlation maps of 12 brain structures with a key role in autonomic regulation were computed for

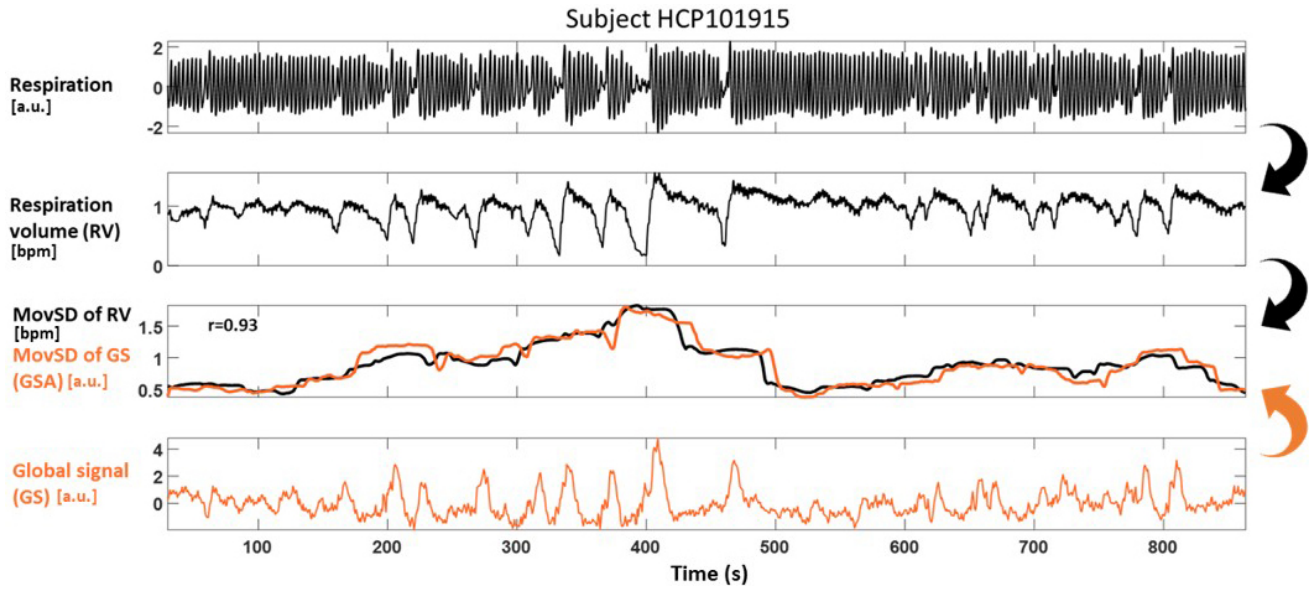

Fig. 2. Experiment 1. Illustration of strong correlation ($r = 0.93$) between global signal amplitude (GSA) and irregularity in breathing for an HCP dataset subject. (1st row) Respiration monitored with respiratory bellows placed around the chest. (2nd row) Respiration volume (RV) defined as the moving standard deviation of respiration using a window length of 6 seconds as in Chang et al. (2009). (3rd row) Moving standard deviation of RV (black line) and global signal (GS; orange line) using a window length of 80 seconds (4th row) FMRI GS defined as the mean time series averaged across all voxels in the grey matter. Note that high values of GSA (e.g., between 200 and 500 seconds) indicate periods with strong fluctuations in RV, whereas low values of GSA (e.g., 500–600 seconds) indicate periods with regular breathing. Resting-state data from HCP subject HCP101915 (Van Essen et al., 2013). For an illustration of the association between GSA and breathing rate, heart rate and PPG amplitude, see Supplementary Figure S2.

all subjects in the low and high state (i.e., considering functional volumes with GSA values in the lowest and highest quartile, respectively). For each of the 12 seeds, 150 principal components were found to explain about 90% of the variance in the correlation maps. Among the 12 seeds, only 3 (anterior insula, PCu/PCC, and cuneus) yielded components for which the weights could discriminate between the 4 groups (i.e., healthy controls, low-risk, high-risk, and SUDEP patients; Fig. 3). More specifically the *F*-statistic, which reflects the degree to which the mean of component weights differed between the four groups, was significant (chance level: $F < 9.4$, corresponding to a *p*-value of 2×10^{-5} under a null distribution of 10,000 permutations) for the following components: anterior insula #3 in the low state ($F = 13.8$, $p < 10^{-7}$), PCu/PCC #2 in the low state ($F = 12.0$, $p < 10^{-6}$), and Cuneus #1 in the high state ($F = 10.2$, $p < 10^{-5}$). Similar results were obtained when excluding data from the two subjects with shorter fMRI scans (Supplementary Fig. S6).

3.2.2. Functional connectivity (FC) patterns and relationship with interval between the time of fMRI scan acquisition and SUDEP

In this section, we examine the FC patterns specific to the three structures identified with significant group differences: anterior insula, PCu/PCC, and cuneus.

3.2.2.1. Anterior insula seed connectivity. Figure 4A shows the mean anterior insula seed-based correlation map (averaged across subjects and time) used as a reference for the interpretation of the different component weights observed across the groups. The anterior insula was positively correlated with the anterior cingulate cortex, regions of the middle frontal gyrus, postcentral gyrus, inferior parietal lobe, and posterior insula, and negatively correlated with the posterior cingulate cortex, and regions of the middle temporal gyrus and frontal gyrus. The FC pattern of component #3 that was the most discriminant principal component of anterior insula exhibited positive weights in the posterior cingulate cortex, and regions of the middle temporal gyrus and frontal gyrus, and negative weights in the anterior cingulate cortex, and anterior and posterior insula (Fig. 4B).

It can be seen that the FC pattern #3 of anterior insula is, to a large degree, the inverse of the anterior insula seed-based correlation map, and thus, a positive weight for the involvement of this pattern on a subject can be interpreted as decline in anterior insula connectivity as compared with the mean connectivity observed in the entire cohort. In other words, both positive and negative correlation values of the anterior insula's connectivity, with the anterior and posterior cingulate cortices, respectively, are weaker. Similarly, a negative weight of FC pattern #3 for within-subject involvement indicates stronger anterior

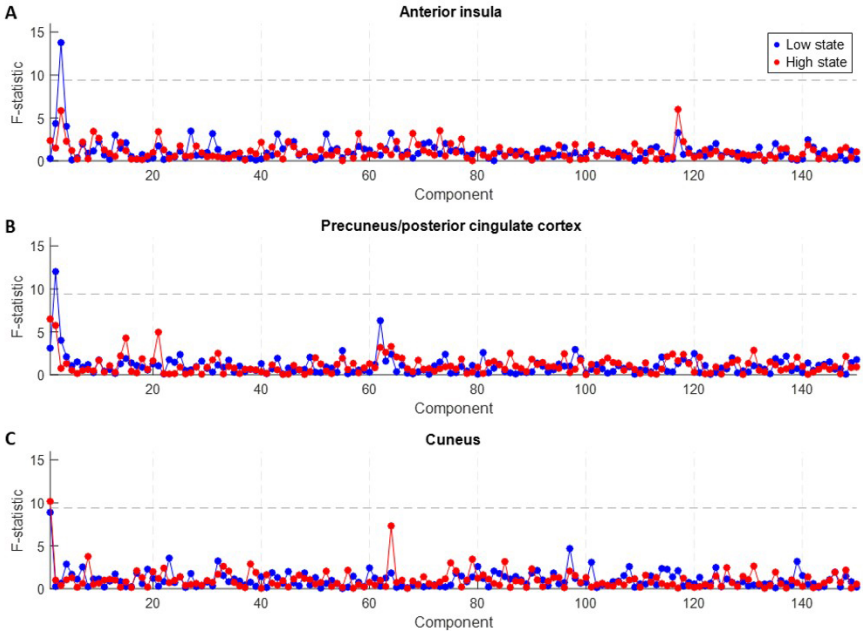

Fig. 3. Experiment 2. *F*-statistics for assessing dispersion between groups based on FC patterns of (A) anterior insula, (B) precuneus/posterior cingulate cortex (PCu/PCC), and (C) cuneus. The dashed line indicates the chance level ($p < 0.05$, Bonferroni corrected), as determined by permutation distribution. All three regions had one of the first three principal components with an *F*-statistic at above chance level. None of the other nine seed regions examined here was found to yield a significant component in terms of *F*-statistic.

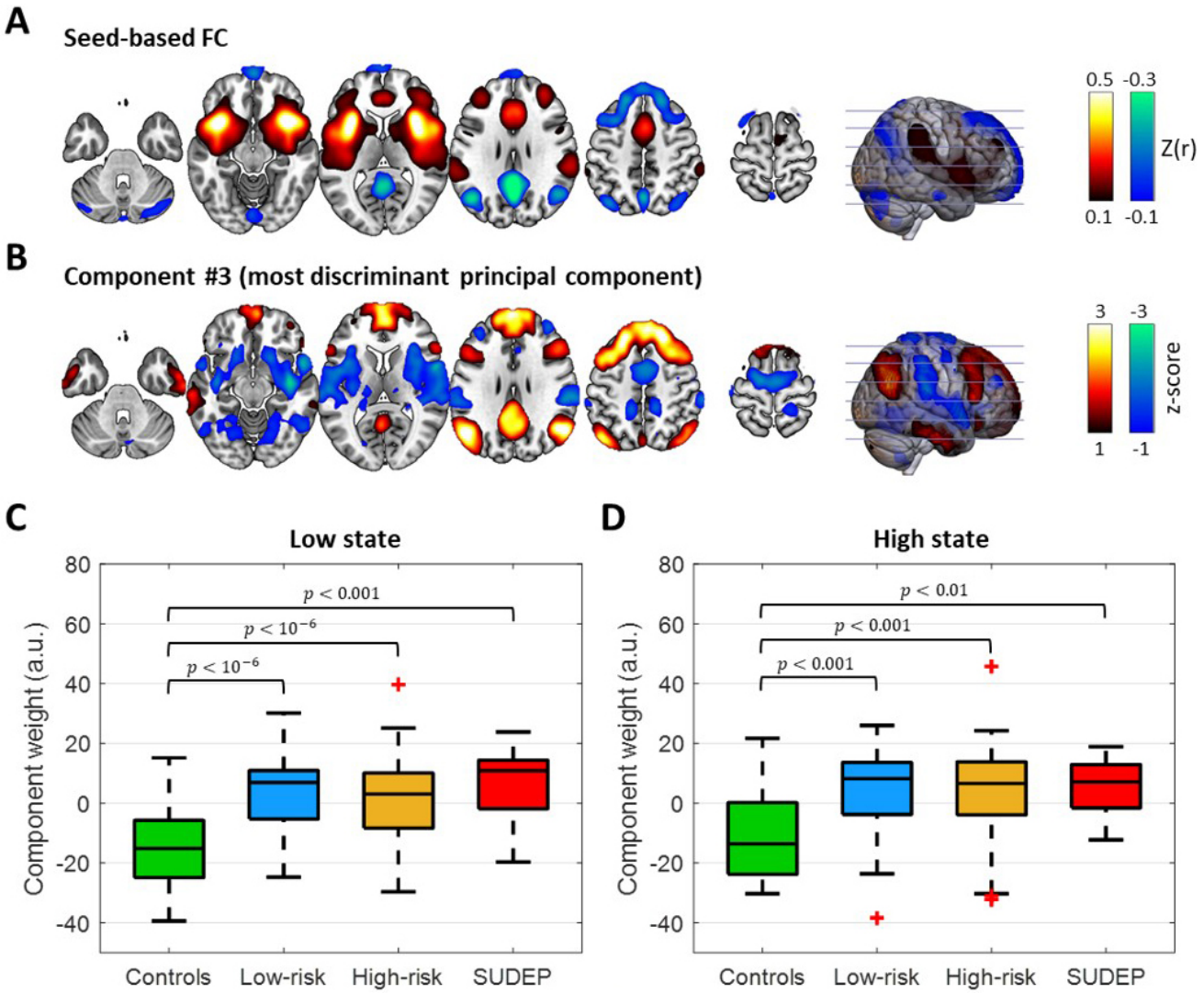

Fig. 4. Experiment 2. Involvement of FC pattern #3 of anterior insula connectivity in the low and high (GSA) states. (A) Seed-based correlation map with the seed placed in the anterior insula averaged across subjects and time. (B) FC pattern of component #3 derived from the anterior insula connectivity profiles of all subjects through PCA. Component weights of the four groups in the (C) low and (D) high state (the bottom and top of each box correspond to the 25th and 75th percentiles of the sample distribution, the line in the box corresponds to the median and the crosses indicate outliers, defined as values that are more than 1.5 times the interquartile range away from the edges of the box). The FC pattern of component #3 was, to a large degree, opposite of the anterior insula connectivity profile. Thus, a positive component weight as found in the epilepsy groups can be interpreted as weakening of the anterior insula connectivity with its typical connections (e.g., anterior and posterior cingulate cortex). For the spatial involvement of large-scale networks in FC pattern #3, see Supplementary Figure S5.

insula connections with respect to the mean connectivity. In both the low and high states, the epilepsy groups were characterized by significantly elevated component weights ($p < 0.01$; Fig. 4C, D). In addition, the majority of individuals with epilepsy were characterized by a positive component weight in contrast to negative component weights for most healthy controls. Furthermore, for the SUDEP cases, the anterior insula FC pattern #3 component weights observed in the high state were found to be strongly negatively correlated with the interval between the fMRI scan and time of SUDEP (r = -0.74, p = 0.02, uncorrected for the six tests performed; Fig. 5), whereas this association was not observed in the low state ($p > 0.05$). A similar strong negative correlation between FC pattern #3 component weights and the interval between the fMRI scan and time of SUDEP was observed in the low state when excluding data from the two subjects with shorter fMRI scans (Supplementary Fig. S7).

3.2.2.2. PCu/PCC seed connectivity. The correlation map of the PCu/PCC averaged across subjects and time consisted of positive correlations with the posterior

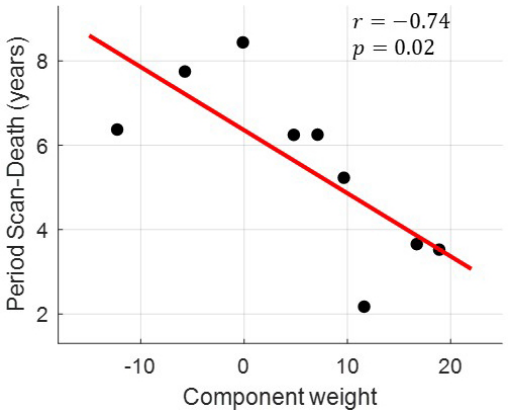

Fig. 5. Experiment 2. Strength of anterior insula connectivity linked to the interval between the fMRI scan and time of SUDEP. The weight of component #3 in the high state (irregular cardiorespiratory activity) decreased with interval length (r = -0.74, p = 0.02). Given that the FC pattern of component #3 (Fig. 4B) is, to a large extent, the inverse of the mean anterior insula connectivity (Fig. 4A), a positive weight for the within-subject involvement can be interpreted as reduced anterior insula connectivity. Thus, the inverse relationship between component weight and scan–SUDEP interval indicates that patients who died relatively soon after the scan exhibited weak anterior insula connectivity.

middle and superior temporal gyri, and the medial frontal gyrus, and negative correlations with the precentral and postcentral gyri, inferior frontal gyrus, anterior superior temporal gyrus, and anterior insula cortex (Supplementary Fig. S3A). The FC pattern of component #2 (most discriminant principal component of PCu/PCC) consisted of positive weights in the precuneus/posterior cingulate cortex, superior occipital cortex, middle temporal gyrus, angular gyrus, and middle and medial frontal gyri (Supplementary Fig. S3B). In addition, it exhibited negative weights in regions close to the cerebral hemispheres and brainstem, such as the amygdala, hippocampus, parahippocampal gyrus, putamen, claustrum, superior temporal gyrus, and fusiform gyrus. In the low state, the three epilepsy groups exhibited significantly reduced weights for component #2 ($p < 0.001$; Supplementary Fig. S3C), with the majority of patients exhibiting negative weights and the majority of controls exhibiting positive weights. Similar observations were made in the high state (Supplementary Fig. S3D). The weights of PCu/PCC component #2 did not show any association with the interval between the fMRI scan and the occurrence of SUDEP.

3.2.2.3. Cuneus seed connectivity. The cuneus correlation map averaged across subjects and time presented negative correlations with the inferior parietal lobe, inferior frontal gyrus, and inferior temporal gyrus (Supplementary Fig. S4A). The FC pattern of component #1 (most discriminant component of cuneus) consisted of positive weights in the ventral anterior cingulate cortex, precentral and postcentral gyrus, superior temporal gyrus, as well as cuneus, and negative weights in the posterior cingulate cortex, regions of the superior and middle temporal gyrus, thalamus, and frontal gyrus (Supplementary Fig. S4B). In the low state, the three epilepsy groups exhibited significantly higher component weights than healthy controls ($p < 0.05$; Supplementary Fig. S4C). The higher component weights of low-risk and high-risk patients as compared with controls were also observed in the high state (Supplementary Fig. S4D). The weights of cuneus component #1 did not show any association with the interval between the fMRI scan and the occurrence of SUDEP.

3.2.2.4. Large-scale network involvement. With regard to the spatial involvement of the Yeo et al. (2011) large-scale networks in the connectivity patterns revealed in this work, the anterior insula component #3 reflected engagement of the anterior insula with regions of the default mode network and, to a lesser degree, frontoparietal network, and disengagement with the ventral attention and somatomotor network (Supplementary Fig. S5). The PCu/PCC component #2 engaged connectivity with regions that partly belong to the default mode network. Although widespread regions of this component were disengaged with the PCu/PCC, they did not resemble any of the large-scale networks. Finally, the cuneus component #1 reflected mainly engagement of the cuneus with regions of the somatomotor network, and disengagement with regions of the default mode network.

4. DISCUSSION

This study utilized resting-state fMRI data to examine FC in patients with drug-resistant epilepsy, some of whom subsequently succumbed to SUDEP. Given the strong link between time-varying FC and variations in autonomic activity (Chang et al., 2013; Mulcahy et al., 2019; Nikolaou et al., 2016), particular attention was placed on characterizing connectivity in periods with regular and irregular cardiorespiratory activity, separately. We also examined whether any of the observed effects are linked to the risk for SUDEP.

We first demonstrated that the moving standard deviation of fMRI global signal, termed here “global signal amplitude” (GSA), is elevated during periods with strong fluctuations in breathing and cardiac activity (Experiment 1) using data in the public domain. Specifically, we showed that GSA is elevated during periods of the order of 1 minute that present at least one of the following features: a transient apnea, variations in respiratory volume,

transient increases in heart rate, or variations in the amplitude of the PPG (Supplementary Fig. S1). In this work, such periods correspond to a "high GSA state". Our study extends previous findings by demonstrating that the association of GSA and variations in cardiorespiratory rhythms previously found across subjects and fMRI runs (Kassinopoulos & Mitsis, 2019; Orban et al., 2020; Power et al., 2017) is also present within a run at the scale of minutes. This finding indicates that previously collected fMRI datasets that did not include monitoring of physiological processes could be revisited to study aspects of the autonomic nervous system. This outcome is particularly relevant for fMRI studies examining rare diseases and phenomena with a low incidence rate, such as SUDEP.

To our knowledge, the approach of using the lowest and highest quartiles of global signal amplitude (GSA) to define discrete physiological states is novel. While prior studies linked GSA to physiological variability, they have not used it to segment fMRI data into distinct states for functional connectivity analysis. We focused on the extreme quartiles to enhance contrast between stable and unstable autonomic conditions, thereby improving interpretability. The middle quartiles were excluded to avoid transitional periods that may introduce physiological heterogeneity. Future work may explore these intermediate states to better understand the full continuum of autonomic dynamics.

Subsequently, we characterized FC in nine SUDEP cases as compared with healthy participants, and patients (alive at the time of this analysis) classified as either at low or high risk of SUDEP based on the frequency of TCS (Experiment 2). Resting-state fMRI scans of 20-minute duration from each subject were considered for connectivity assessment in the "low GSA state" and "high GSA state". Seed-based connectivity analysis was employed, focusing on 12 brain structures with key roles in autonomic and respiratory regulation. The seed-based correlation maps were further analysed with PCA to summarize differences in connectivity between the groups and states in terms of a few components that explain most of the variance in the data.

Consistent with previous studies (Chang & Glover, 2009; Deen et al., 2011; Seeley et al., 2007; Uddin et al., 2009), activity in the anterior insula was positively correlated with that in the anterior cingulate cortex and inferior parietal lobe ("anterior insula positive network"), and negatively correlated with PCu/PCC and lateral parietal cortices ("anterior insula negative network"; Fig. 4A). However, our analysis yielded an FC pattern (in the form of the 3rd principal component) with a spatial map that is, to a large extent, the inverse of the mean anterior insula connectivity (Fig. 4B) and whose involvement in epilepsy patients was relatively high (Fig. 4C, D). This finding indicates weaker anterior insula networks in epilepsy patients compared with healthy controls. Furthermore, this weakening was more pronounced in the low state (characterized by more regular cardiac and breathing activity).

The findings also showed that the connectivity of cuneus and PCu/PCC is altered in epilepsy patients (low- and high-risk patients and SUDEP cases; Supplementary Figs. S3 and S4), which is in line with previous findings (Kay et al., 2013; Luo et al., 2012; Rajpoot et al., 2015). However, we found no evidence specifically implicating the aforementioned regions in SUDEP. Namely, the principal components that discriminated epilepsy patients from healthy controls did not reveal significant differences between SUDEP cases and low- or high-risk patients.

4.1. Relationship of anterior insula connectivity with survival time from fMRI scan

The observation of a negative correlation between the strength of anterior insula connectivity during the high state (irregular cardiorespiratory activity) and the interval between the fMRI scan and time of SUDEP may point to a predictive marker. Specifically, we found that patients who died sooner after the fMRI scan (2–4 years post-scan) exhibited lower anterior insula connectivity than patients who died later (5–8 years post-scan; $p = 0.02$, uncorrected; N = 9; Fig. 5). While this outcome suggests an important dysfunctional role specific to the insula in SUDEP, it should be pointed out that the strength of anterior insula connectivity with its associated positive and negative networks was similar in SUDEP cases to that for low- and high-risk patients. Therefore, it is likely that other factors are required to coexist with weak connectivity in the anterior insula to predispose individuals with epilepsy to SUDEP.

The anterior insula plays a major role in cardiovascular and respiratory functions, and has reciprocal connections with several limbic structures, including the anterior cingulate cortex, amygdala, and hypothalamus (Palma & Benarroch, 2014). It receives viscerosensory inputs and, through its projections to brainstem output nuclei, contributes to regulation of blood pressure and other autonomic responses (Benarroch, 1993; Palma & Benarroch, 2014; Ruggiero et al., 1987; Saper, 1982; Stephen Oppenheimer & Cechetto, 2016). Functional imaging studies consistently report activation of the anterior insula in a wide range of interoceptive stimuli including dyspnea, "air hunger" and heartbeat awareness, as well as in emotional processing (Brannan et al., 2001; Craig, 2009; Harrison et al., 2021; Zaki et al., 2012). In epilepsy, it has been suggested that seizures may affect insula

activity leading to respiratory depression and cardiac arrhythmia, thereby increasing the risk of SUDEP (Li et al., 2017; S. Oppenheimer, 2001). However, scalp EEG, as used typically in the clinic for detecting seizures, has poor sensitivity to electrical activity from deep structures such as the insula and, consequently, it is difficult to assess whether seizure-induced autonomic manifestations are caused by insular dysfunction (Stephen Oppenheimer & Cechetto, 2016).

Altered FC between the insula and cingulate cortex in SUDEP and high-risk cases has been previously shown (Allen, Harper, et al., 2019), which is in line with our findings. In addition, patients who died of SUDEP at a time close to a structural MRI scan exhibited increased volume of the anterior insula (Allen, Vos, et al., 2019), further supporting the notion that impairment in the anterior insula may contribute to SUDEP. Finally, we recently found, in epilepsy patients, abnormal connectivity of the insula with the thalamus relative to changes in cardiac rhythms (Kassinopoulos et al., 2021). Collectively, these findings suggest that, in epilepsy, communication of the anterior insula with other regions of the central nervous system may deteriorate over time, potentially leading to increased risk of cardiac or respiratory failure.

While anterior insula connectivity did not significantly differ between SUDEP and non-SUDEP epilepsy patients, we observed a strong inverse correlation between connectivity strength and the interval between the fMRI scan and SUDEP occurrence. This association was only present during periods of irregular cardiorespiratory activity (high GSA state), suggesting that anterior insula dysfunction may be particularly relevant under autonomic stress. Importantly, the distribution of connectivity values across the epilepsy cohort indicates that reduced anterior insula connectivity is not unique to SUDEP cases. This implies that while insula dysfunction may reflect a vulnerability factor, it is likely not sufficient on its own to predict SUDEP. Instead, the dysfunction may need to coexist with other, SUDEP-specific mechanisms to contribute to the fatal outcome. In this context, recent findings showing that post-convulsive bradycardia and exaggerated sinus arrhythmia with bradycardia are overrepresented in SUDEP cases (Vilella et al., 2024) underscore the potential role of peri-ictal autonomic instability in SUDEP pathophysiology.

4.2. Impaired communication between ventral and default mode network in epilepsy patients

We observed that activity in the anterior insula is positively correlated with that in regions of the ventral network and negatively correlated with regions of the default mode network (Fig. 4), and that this effect is weaker in patients with epilepsy, and is linked to SUDEP (Fig. 5). Seeley et al. (2007) first identified the so-called ventral network (also known as salience network) consisting of the anterior insula and anterior cingulate cortex as well as subcortical and limbic structures, with their activity linked to measures of anxiety. Subsequent functional studies implicated ventral attention regions mediating sympathetic activity (Beissner et al., 2013). Similarly, regions of the default mode network, including the posterior cingulate cortex, were found to be associated with parasympathetic activity (Beissner et al., 2013). Sridharan et al. (2008) demonstrated that the salience network, and particularly the anterior insula, is responsible for reducing activity in the default mode network during goal-directed tasks. Initial studies attributed autonomic dysfunction in epilepsy to seizures originating from, or spreading to, individual regions such as the anterior insula (S. Oppenheimer, 2001) and anterior cingulate cortex (Devinsky et al., 1995). However, our results suggest also the possibility that cardiorespiratory failure may rise from impaired communication between the ventral and default mode network due to insula dysfunction which could also explain the alteration in parasympathetic and sympathetic activity observed often in individuals with epilepsy (Myers et al., 2018).

The use of the mean grey matter signal (global signal) as a nuisance regressor may appear counterintuitive in a study investigating autonomic and breathing influences on functional connectivity, given that the global signal reflects fluctuations related to heart rate and breathing patterns. However, this approach is justified by the fact that the global signal predominantly captures widespread physiological artefacts, which are often driven by systemic vascular fluctuations rather than localized neural activity. These artefacts can obscure true neural connectivity patterns, particularly in regions with dense vasculature. Therefore, regressing out the global signal helps mitigate these confounds and enhances the specificity of functional connectivity estimates. While the global signal is used here to reduce physiological noise, we also recognize its interpretive value. Specifically, fluctuations in the amplitude of the global signal, as captured by the global signal amplitude (GSA), reflect systemic physiological changes, including variations in heart rate and breathing patterns. These autonomic modulations can, in principle, coincide with changes in neural-driven functional connectivity. Thus, although the global signal is regressed out to mitigate widespread physiological artefacts, its amplitude remains a valuable tool for identifying periods of altered autonomic state, which may help uncover state-dependent neural connectivity patterns relevant to SUDEP.

4.3. Limitations and possible future work

Our study has a number of limitations. The unavailability of concurrent PPG and respiratory belt recordings led us in using GSA as a probe of cardiac and breathing activity. Although GSA reflects physiological changes, it cannot distinguish between irregular cardiovascular (transient increase in heart rate, variations in PPG amplitude, variations in blood pressure) and breathing (transient apnea, variations in tidal volume, etc.), with possible loss of sensitivity. Moreover, the relationship between GSA and physiological variability, as established in healthy individuals (Experiment 1), may not fully generalize to epilepsy patients. Differences in autonomic regulation, seizure-related effects, or medication use could alter the physiological underpinnings of GSA in this population. This limitation should be taken into account when interpreting the findings. It is also important to note that prior studies have shown that respiratory signals can exert a particularly strong influence on brain activity, particularly in limbic and autonomic regions (Kananen et al., 2022; Wu et al., 2015; Zelano et al., 2016). As such, respiratory dynamics play a dominant role in shaping the observed brain states in our analysis. For most witnessed SUDEP events, a TCS is observed a few minutes before death which triggers abnormal breathing patterns followed by episodes of bradycardia and terminal asystole, pointing to possible future studies focused on the link between irregular breathing and brain connectivity.

While some scans showed relatively strong correlations between GSA and individual physiological variables, in most cases, the correlations were of low to moderate strength. This outcome likely reflects the multifactorial nature of the GS, which is influenced not only by physiological processes, but also by motion, neural activity, and potential noise in the physiological recordings.

Another physiological factor not accounted for in the analysis was epileptiform activity. Epileptic discharges may directly influence cardiovascular rhythms and their neural correlates, potentially interacting with GSA-derived signals and FC patterns. Although EEG data were acquired alongside fMRI, a detailed inspection of epileptiform events has not yet been performed. Nevertheless, subjects with frequent epileptiform spikes were excluded based on preliminary EEG review. A comprehensive evaluation by a clinical neurophysiologist remains a key component of our planned future work.

Another important consideration is the potential decline in vigilance during resting-state fMRI sessions. Prior studies have shown that arousal levels often decrease within the first 5–10 minutes of scanning, leading to systematic changes in fMRI signals, functional connectivity, and global signal amplitude (Bijsterbosch et al., 2017; Orban et al., 2020; Tagliazucchi & Laufs, 2014). Although EEG was not available in the HCP dataset to confirm wakefulness, and sleep staging was not performed in our dataset, the observed amplitude changes over time may reflect such vigilance-related effects. While these fluctuations introduce variability, they may also offer a window into the physiological processes that modulate brain–body interactions. Future studies incorporating EEG-based sleep staging will be essential to disentangle the contributions of arousal and sleep to the observed dynamics.

Our data were collected during daytime. SUDEP often occurs at night, and likely during sleep, when physiological processes change (e.g., heart and respiratory rates initially decline, but then increase and become more variable on entering rapid eye movement sleep; Purnell et al., 2018). Given these changes, in the present study, we sought to assess FC at different physiological states. However, the increased risk of SUDEP at night may result from other factors such as the influence of circadian rhythms and sleep on the brain, which could not be studied here since the fMRI data had been collected during daytime in a resting condition. While studying FC during sleep could help us understand the mechanisms underlying cardiorespiratory dysfunction, such studies are rare, as sleeping inside the scanner overnight is not well tolerated by participants. Therefore, fMRI studies need to consider protocols which mimic conditions that likely contribute to cardiorespiratory failure, while also being safe and practical. An example of such a test is the hypercapnic ventilatory response which was shown by Sainju et al. (2019) to indicate individuals with a prolonged increase in post-ictal CO_2 after TCS, who are arguably at a high risk of SUDEP. Future fMRI studies may need to consider breathing or cardiovascular challenges during scans, along with physiological monitoring, to better understand how regional brain areas respond to such manipulation in patients at risk for SUDEP.

Another important limitation is the heterogeneity of our sample, which included individuals with different epilepsy syndromes and etiologies. This issue was largely due to the relative rarity of SUDEP cases who have undergone fMRI, which necessitated a broader recruitment strategy to ensure sufficient sample size for meaningful analysis. Additionally, while the frequency of TCS could, in principle, be treated as a continuous variable to explore associations with connectivity measures, we opted for a categorical classification due to inconsistencies in seizure documentation across patients. We also did not examine the influence of the epileptogenic hemisphere on connectivity patterns, as lateralization data were not consistently available across the cohort. Future studies with more standardized and granular clinical information,

including seizure frequency, lateralization, and etiology, may enable more refined analyses of SUDEP risk factors.

We also acknowledge that the brainstem and midcingulate cortex, despite their established roles in autonomic regulation (Ferraro et al., 2022), were not included as seed regions due to the poor signal-to-noise ratio observed in our 3T fMRI data in brainstem and the need to limit the number of statistical comparisons. Future studies with optimized acquisition protocols and larger sample sizes may help clarify the contribution of these regions to SUDEP risk.

Moreover, in this study, we included global signal regression (GSR) to mitigate widespread physiological noise (Kassinopoulos & Mitsis, 2021; Xifra-Porxas et al., 2021), with the aim of enhancing sensitivity to subtle effects of autonomic activity. However, given the ongoing debate in the field and concerns that GSR may inadvertently remove signal related to vigilance or neural processes, we repeated the key analyses without applying GSR. As anticipated, the results differed: of the three seed-based connectivity components that initially discriminated between groups, only one (PCu/PCC) retained a component with an *F*-statistic above chance level (Supplementary Figs. S8 and S9). While we maintain that GSR is a reasonable approach for reducing global physiological confounds, further work is needed to evaluate its appropriateness in studies investigating autonomic influences on brain connectivity.

Finally, although our data suggest that the strength of anterior insula connectivity is inversely proportional to the interval between the fMRI scan and time of SUDEP (r = -0.74; p = 0.02, uncorrected; N = 9; Fig. 5), this finding is based solely on cross-sectional data and, thus, should be interpreted with caution. Longitudinal data, ideally incorporating postmortem data, may help clarify whether insular dysfunction progresses over time and how it relates to neuropathological findings in SUDEP (e.g., Nascimento et al., 2017).

5. CONCLUSIONS

In this work, we revealed altered FC patterns of cuneus and precuneus/posterior cingulate cortex in epilepsy as compared with healthy controls during periods of regular cardiorespiratory rhythms. These findings were based on the use of global signal amplitude (GSA), which we showed to be a marker of cardiorespiratory rhythm irregularity (transient apnea, transient increase in heart rate, etc.). In addition, we found reduced anterior insula connectivity in epilepsy, particularly during periods of regular cardiac and breathing activity. For SUDEP cases, the insular connectivity effect was inversely correlated with the scan–SUDEP interval. Overall, our results suggest that connectivity measures of the anterior insula may represent a contributing factor to SUDEP risk, rather than a standalone biomarker, as similar connectivity patterns were also observed in non-SUDEP epilepsy patients. Future research efforts should focus on gaining insight into the role of anterior insula connectivity in seizure-induced cardiorespiratory failure and how intervention strategies could be employed to restore anterior insula function.

DATA AND CODE AVAILABILITY

The data used for image processing and generating the results presented in this manuscript are not publicly accessible due to patient confidentiality, ethical restrictions, and UK National Health Service data protection regulations.

AUTHOR CONTRIBUTIONS

Conceptualization: M.K., R.M.H., L.R.K., M.G., L.L., B.D; data curation: M.K., N.R., L.A., J.O., C.S., L.L., B.D; formal analysis: M.K., L.A., J.O., C.S., L.L., B.D; funding acquisition: R.M.H., L.R.K., L.L., B.D; investigation: M.K., R.M.H., C.S., M.G., L.L., B.D; methodology: M.K., M.G., L.L., B.D; project administration: M.K., L.L., B.D; resources: M.K., L.L., B.D; software: M.K.; supervision: M.K., L.L., B.D; validation: M.K.; visualization: M.K., N.R.; writing—original draft: M.K.; writing—review & editing: M.K., N.R., R.M.H., J.O., C.S., L.R.K., M.G., L.L., B.D. All authors read and approved the final manuscript.

FUNDING

This work was funded by Epilepsy Research UK (Grant number: P1905). Funding by the NIH—National Institute of Neurological Disorders and Stroke (The Center for SUDEP Research; Grant number: U01-NS090407) and Hungarian NRDIO (National Research, Development, and Innovation Office; Grant number: OTKA K128040) is also acknowledged. This work was supported by the National Institute for Health Research University College London Hospitals Biomedical Research Centre.

DECLARATION OF COMPETING INTEREST

The authors declare no conflict of interest.

ACKNOWLEDGMENTS

We thank Luke Allen for his assistance with data curation and are grateful to the Epilepsy Society for supporting the Epilepsy Society MRI scanner used in this study.

SUPPLEMENTARY MATERIALS

Supplementary material for this article is available with the online version here: https://doi.org/10.1162/IMAG.a.918.

REFERENCES

Ali, A., Wu, S., Issa, N. P., Rose, S., Towle, V. L., Warnke, P., & Tao, J. X. (2017). Association of sleep with sudden unexpected death in epilepsy. *Epilepsy and Behavior*, *76*, 1–6. https://doi.org/10.1016/j.yebeh.2017.08.021

Allen, L. A., Harper, R. M., Guye, M., Kumar, R., Ogren, J., Vos, S., Ourselin, S., Scott, C., Lhatoo, S., Lemieux, L., & Diehl, B. (2019). Altered brain connectivity in sudden unexpected death in epilepsy (SUDEP) revealed using resting-state fMRI. *NeuroImage: Clinical*, *24*, 102060. https://doi.org/10.1016/j.nicl.2019.102060

Allen, L. A., Harper, R. M., Kumar, R., Guye, M., Ogren, J. A., Lhatoo, S. D., Lemieux, L., Scott, C. A., Vos, S. B., Rani, S., & Diehl, B. (2017). Dysfunctional brain networking among autonomic regulatory structures in temporal lobe epilepsy patients at High Risk of sudden unexpected death in epilepsy. *Frontiers in Neurology*, *8*, 1–13. https://doi.org/10.3389/fneur.2017.00544

Allen, L. A., Vos, S. B., Kumar, R., Ogren, J. A., Harper, R. K., Winston, G. P., Balestrini, S., Wandschneider, B., Scott, C. A., Ourselin, S., Duncan, J. S., Lhatoo, S. D., Harper, R. M., & Diehl, B. (2019). Cerebellar, limbic, and midbrain volume alterations in sudden unexpected death in epilepsy. *Epilepsia*, *60*(4), 718–729. https://doi.org/10.1111/epi.14689

Arbune, A. A., Jeppesen, J., Conradsen, I., Ryvlin, P., & Beniczky, S. (2020). Peri-ictal heart rate variability parameters as surrogate markers of seizure severity. *Epilepsia*, *61*(Suppl. 1), S55–S60. https://doi.org/10.1111/epi.16491

Behzadi, Y., Restom, K., Liau, J., & Liu, T. T. (2007). A component based noise correction method (CompCor) for BOLD and perfusion based fMRI. *NeuroImage*, *37*(1), 90–101. https://doi.org/10.1016/j.neuroimage.2007.04.042

Beissner, F., Meissner, K., Bar, K.-J., & Napadow, V. (2013). The autonomic brain: An activation likelihood estimation meta-analysis for central processing of autonomic function. *Journal of Neuroscience*, *33*(25), 10503–10511. https://doi.org/10.1523/JNEUROSCI.1103-13.2013

Benarroch, E. E. (1993). The central autonomic network: Functional organization, dysfunction, and perspective. *Mayo Clinic Proceedings*, *68*(10), 988–1001. https://doi.org/10.1016/S0025-6196(12)62272-1

Bijsterbosch, J., Harrison, S., Duff, E., Alfaro-Almagro, F., Woolrich, M., & Smith, S. (2017). Investigations into within- and between-subject resting-state amplitude variations. *NeuroImage*, *159*, 57–69. https://doi.org/10.1016/j.neuroimage.2017.07.014

Brannan, S., Liotti, M., Egan, G., Shade, R., Madden, L., Robillard, R., Abplanalp, B., Stofer, K., Denton, D., & Fox, P. T. (2001). Neuroimaging of cerebral activations and deactivations associated with hypercapnia and hunger for air. *Proceedings of the National Academy of Sciences of the United States of America*, *98*(4), 2029–2034. https://doi.org/10.1073/pnas.98.4.2029

Chang, C., Cunningham, J. P., & Glover, G. H. (2009). Influence of heart rate on the BOLD signal: The cardiac response function. *NeuroImage*, *44*(3), 857–869. https://doi.org/10.1016/j.neuroimage.2008.09.029

Chang, C., & Glover, G. H. (2009). Effects of model-based physiological noise correction on default mode network anti-correlations and correlations. *NeuroImage*, *47*(4), 1448–1459. https://doi.org/10.1016/j.neuroimage.2009.05.012

Chang, C., & Glover, G. H. (2010). Time-frequency dynamics of resting-state brain connectivity measured with fMRI. *NeuroImage*, *50*(1), 81–98. https://doi.org/10.1016/j.neuroimage.2009.12.011

Chang, C., Metzger, C. D., Glover, G. H., Duyn, J. H., Heinze, H.-J. J., & Walter, M. (2013). Association between heart rate variability and fluctuations in resting-state functional connectivity. *NeuroImage*, *68*, 93–104. https://doi.org/10.1016/j.neuroimage.2012.11.038

Coan, A. C., Chaudhary, U. J., Grouiller, F., Campos, B. M., Perani, S., De Ciantis, A., Vulliemoz, S., Diehl, B., Beltramini, G. C., Carmichael, D. W., Thornton, R. C., Covolan, R. J., Cendes, F., & Lemieux, L. (2016). EEG-fMRI in the presurgical evaluation of temporal lobe epilepsy. *Journal of Neurology, Neurosurgery and Psychiatry*, *87*(6), 642–649. https://doi.org/10.1136/jnnp-2015-310401

Craig, A. D. B. (2009). How do you feel—Now? The anterior insula and human awareness. *Nature Reviews Neuroscience*, *10*(1), 59–70. https://doi.org/10.1038/nrn2555

Critchley, H. D., Mathias, C. J., Josephs, O., O'Doherty, J., Zanini, S., Dewar, B. K., Cipolotti, L., Shallice, T., & Dolan, R. J. (2003). Human cingulate cortex and autonomic control: Converging neuroimaging and clinical evidence. *Brain*, *126*(10), 2139–2152. https://doi.org/10.1093/brain/awg216

Deen, B., Pitskel, N. B., & Pelphrey, K. A. (2011). Three systems of insular functional connectivity identified with cluster analysis. *Cerebral Cortex*, *21*(7), 1498–1506. https://doi.org/10.1093/cercor/bhq186

DeGiorgio, C. M., Miller, P., Meymandi, S., Chin, A., Epps, J., Gordon, S., Gornbein, J., & Harper, R. M. (2010). RMSSD, a measure of vagus-mediated heart rate variability, is associated with risk factors for SUDEP: The SUDEP-7 Inventory. *Epilepsy and Behavior*, *19*(1), 78–81. https://doi.org/10.1016/j.yebeh.2010.06.011

Devinsky, O., Hesdorffer, D. C., Thurman, D. J., Lhatoo, S., & Richerson, G. (2016). Sudden unexpected death in epilepsy: Epidemiology, mechanisms, and prevention. *The Lancet Neurology*, *15*(10), 1075–1088. https://doi.org/10.1016/S1474-4422(16)30158-2

Devinsky, O., Morrell, M. J., & Vogt, B. A. (1995). Contributions of anterior cingulate cortex to behaviour. *Brain*, *118*(1), 279–306. https://doi.org/10.1093/brain/118.1.279

Devinsky, O., & Sisodiya, S. M. (2020). SUDEP: Advances and challenges. *Epilepsy Currents*, *20*(6 Suppl.), 29S–31S. https://doi.org/10.1177/1535759720947438

Du, Y., Pearlson, G. D., Lin, D., Sui, J., Chen, J., Salman, M., Tamminga, C. A., Ivleva, E. I., Sweeney, J. A., Keshavan, M. S., Clementz, B. A., Bustillo, J., & Calhoun, V. D. (2017). Identifying dynamic functional connectivity biomarkers using GIG-ICA: Application to schizophrenia, schizoaffective disorder, and psychotic bipolar disorder. *Human Brain Mapping*, *38*(5), 2683–2708. https://doi.org/10.1002/hbm.23553

Fan, L., Li, H., Zhuo, J., Zhang, Y., Wang, J., Chen, L., Yang, Z., Chu, C., Xie, S., Laird, A. R., Fox, P. T., Eickhoff, S. B., Yu, C., & Jiang, T. (2016). The human brainnetome atlas: A new brain atlas based on connectional architecture. *Cerebral Cortex*, *26*(8), 3508–3526. https://doi.org/10.1093/cercor/bhw157

Ferraro, S., Klugah-Brown, B., Tench, C. R., Bazinet, V., Bore, M. C., Nigri, A., Demichelis, G., Bruzzone, M. G., Palermo, S., Zhao, W., Yao, S., Jiang, X., Kendrick, K. M., & Becker, B. (2022). The central autonomic system revisited—Convergent evidence for a regulatory role of the insular and midcingulate cortex from neuroimaging meta-analyses. *Neuroscience and Biobehavioral Reviews*, *142*, 104915. https://doi.org/10.1016/j.neubiorev.2022.104915

Fisher, R. S., Cross, J. H., French, J. A., Higurashi, N., Hirsch, E., Jansen, F. E., Lagae, L., Moshé, S. L., Peltola, J., Roulet Perez, E., Scheffer, I. E., & Zuberi, S. M. (2017). Operational classification of seizure types by the International League Against Epilepsy: Position paper of the ILAE commission for classification and terminology. *Epilepsia*, *58*(4), 522–530. https://doi.org/10.1111/epi.13670

Friston, K. J., Ashburner, J., Kiebel, S. J., Nichols, T. E., & Penny, W. D. (Eds.). (2007). *Statistical parametric mapping: The analysis of functional brain images*. Academic Press. http://store.elsevier.com/product.jsp?isbn=9780123725608

Haimovici, A., Tagliazucchi, E., Balenzuela, P., & Laufs, H. (2017). On wakefulness fluctuations as a source of BOLD functional connectivity dynamics. *Scientific Reports*, *7*(1), 1–13. https://doi.org/10.1038/s41598-017-06389-4

Harrison, O. K., Nanz, L., Marino, S., Lüchinger, R., Hennel, F., Hess, A. J., Frässle, S., Iglesias, S., Vinckier, F., Petzschner, F. H., Harrison, S. J., Stephan, K. E., Harrison, O. K., Köchli, L., Marino, S., Luechinger, R., Hennel, F., Brand, K., Hess, A. J., … Stephan, K. E. (2021). Interoception of breathing and its relationship with anxiety. *Neuron*, *109*(24), 4080.e8–4093.e8. https://doi.org/10.1016/j.neuron.2021.09.045

Kananen, J., Järvelä, M., Korhonen, V., Tuovinen, T., Huotari, N., Raitamaa, L., Helakari, H., Väyrynen, T., Raatikainen, V., Nedergaard, M., Ansakorpi, H., Jacobs, J., LeVan, P., & Kiviniemi, V. (2022). Increased interictal synchronicity of respiratory related brain pulsations in epilepsy. *Journal of Cerebral Blood Flow and Metabolism*, *42*(10), 1840–1853. https://doi.org/10.1177/0271678X221099703

Kassinopoulos, M., Harper, R. M., Guye, M., Lemieux, L., & Diehl, B. (2021). Altered relationship between heart rate variability and fMRI-based functional connectivity in people with epilepsy. *Frontiers in Neurology*, *12*, 1–13. https://doi.org/10.3389/fneur.2021.671890

Kassinopoulos, M., & Mitsis, G. D. (2019). Identification of physiological response functions to correct for fluctuations in resting-state fMRI related to heart rate and respiration. *NeuroImage*, *202*, 116150. https://doi.org/10.1016/j.neuroimage.2019.116150

Kassinopoulos, M., & Mitsis, G. D. (2021). Physiological noise modeling in fMRI based on the pulsatile component of photoplethysmograph. *NeuroImage*, *242*, 118467. https://doi.org/10.1016/j.neuroimage.2021.118467

Kassinopoulos, M., & Mitsis, G. D. (2022). A multi-measure approach for assessing the performance of fMRI preprocessing strategies in resting-state functional connectivity. *Magnetic Resonance Imaging*, *85*, 228–250. https://doi.org/10.1016/j.mri.2021.10.028

Kay, B. P., Difrancesco, M. W., Privitera, M. D., Gotman, J., Holland, S. K., & Szaflarski, J. P. (2013). Reduced default mode network connectivity in treatment-resistant idiopathic generalized epilepsy. *Epilepsia*, *54*(3), 461–470. https://doi.org/10.1111/epi.12057

Keller, A. E., Whitney, R., Li, S. A., Pollanen, M. S., & Donner, E. J. (2018). Incidence of sudden unexpected death in epilepsy in children is similar to adults. *Neurology*, *91*(2), e107–e111. https://doi.org/10.1212/WNL.0000000000005762

Kozák, L. R., van Graan, L. A., Chaudhary, U. J., Szabó, Á. G., & Lemieux, L. (2017). ICN_Atlas: Automated description and quantification of functional MRI activation patterns in the framework of intrinsic connectivity networks. *NeuroImage*, *163*, 319–341. https://doi.org/10.1016/j.neuroimage.2017.09.014

Lacuey, N., Hampson, J. P., Theeranaew, W., Zonjy, B., Vithala, A., Hupp, N. J., Loparo, K. A., Miller, J. P., & Lhatoo, S. D. (2018). Cortical structures associated with human blood pressure control. *JAMA Neurology*, *75*(2), 194–202. https://doi.org/10.1001/jamaneurol.2017.3344

Leonardi, N., Richiardi, J., Gschwind, M., Simioni, S., Annoni, J. M., Schluep, M., Vuilleumier, P., & Van De Ville, D. (2013). Principal components of functional connectivity: A new approach to study dynamic brain connectivity during rest. *NeuroImage*, *83*, 937–950. https://doi.org/10.1016/j.neuroimage.2013.07.019

Leonardi, N., & Van De Ville, D. (2015). On spurious and real fluctuations of dynamic functional connectivity during rest. *NeuroImage*, *104*, 430–436. https://doi.org/10.1016/j.neuroimage.2014.09.007

Li, J., Ming, Q., & Lin, W. (2017). The insula lobe and sudden unexpected death in epilepsy: A hypothesis. *Epileptic Disorders*, *19*(1), 10–14. https://doi.org/10.1684/epd.2017.0890

Luo, C., Qiu, C., Guo, Z., Fang, J., Li, Q., Lei, X., Xia, Y., Lai, Y., Gong, Q., Zhou, D., & Yao, D. (2012). Disrupted functional brain connectivity in partial epilepsy: A resting-state fMRI study. *PLoS One*, *7*(1), 15–19. https://doi.org/10.1371/journal.pone.0028196

Macey, P. M., Macey, K. E., Kumar, R., & Harper, R. M. (2004). A method for removal of global effects from fMRI time series. *NeuroImage*, *22*(1), 360–366. https://doi.org/10.1016/j.neuroimage.2003.12.042

Mueller, S. G., Nei, M., Bateman, L. M., Knowlton, R., Laxer, K. D., Friedman, D., Devinsky, O., & Goldman, A. M. (2018). Brainstem network disruption: A pathway to sudden unexplained death in epilepsy? *Human Brain Mapping*, *39*(12), 4820–4830. https://doi.org/10.1002/hbm.24325

Mulcahy, J. S., Larsson, D. E. O., Garfinkel, S. N., & Critchley, H. D. (2019). Heart rate variability as a biomarker in health and affective disorders: A perspective on neuroimaging studies. *NeuroImage*, *202*, 116072. https://doi.org/10.1016/j.neuroimage.2019.116072

Myers, K. A., Sivathamboo, S., & Perucca, P. (2018). Heart rate variability measurement in epilepsy: How can we move from research to clinical practice? *Epilepsia*, *59*(12), 2169–2178. https://doi.org/10.1111/epi.14587

Nascimento, F. A., Tseng, Z. H., Palmiere, C., Maleszewski, J. J., Shiomi, T., McCrillis, A., & Devinsky, O. (2017). Pulmonary and cardiac pathology in sudden unexpected death in epilepsy (SUDEP). *Epilepsy & Behavior*, *73*, 119–125. https://doi.org/10.1016/j.yebeh.2017.05.013

Nashef, L., So, E. L., Ryvlin, P., & Tomson, T. (2012). Unifying the definitions of sudden unexpected death in epilepsy. *Epilepsia*, *53*(2), 227–233. https://doi.org/10.1111/j.1528-1167.2011.03358.x

Nikolaou, F., Orphanidou, C., Papakyriakou, P., Murphy, K., Wise, R. G., & Mitsis, G. D. (2016). Spontaneous physiological variability modulates dynamic functional connectivity in resting-state functional magnetic resonance imaging. *Philosophical Transactions. Series A, Mathematical, Physical, and Engineering Sciences*, *374*(2067), 20150183-. https://doi.org/10.1098/rsta.2015.0183

Oppenheimer, S. (2001). Forebrain lateralization and the cardiovascular correlates of epilepsy. *Brain*, *124*(12), 2345–2346. https://doi.org/10.1093/brain/124.12.2345

Oppenheimer, S., & Cechetto, D. (2016). The insular cortex and the regulation of cardiac function. *Comprehensive Physiology*, *6*(2), 1081–1133. https://doi.org/10.1002/cphy.c140076

Orban, C., Kong, R., Li, J., Chee, M. W. L., & Yeo, B. T. T. (2020). Time of day is associated with paradoxical reductions in global signal fluctuation and functional connectivity. *PLoS Biology*, *18*(2), e3000602. https://doi.org/10.1371/journal.pbio.3000602

Palma, J. A., & Benarroch, E. E. (2014). Neural control of the heart: Recent concepts and clinical correlations. *Neurology*, *83*(3), 261–271. https://doi.org/10.1212/WNL.0000000000000605

Power, J. D., Barnes, K. A., Snyder, A. Z., Schlaggar, B. L., & Petersen, S. E. (2012). Spurious but systematic correlations in functional connectivity MRI networks arise from subject motion. *NeuroImage*, *59*(3), 2142–2154. https://doi.org/10.1016/j.neuroimage.2011.10.018

Power, J. D., Plitt, M., Laumann, T. O., & Martin, A. (2017). Sources and implications of whole-brain fMRI signals in humans. *NeuroImage*, *146*, 609–625. https://doi.org/10.1016/j.neuroimage.2016.09.038

Power, J. D., Schlaggar, B. L., & Petersen, S. E. (2015). Recent progress and outstanding issues in motion correction in resting state fMRI. *NeuroImage*, *105*, 536–551. https://doi.org/10.1016/j.neuroimage.2014.10.044

Preti, M. G., Bolton, T. A., & Van De Ville, D. (2017). The dynamic functional connectome: State-of-the-art and perspectives. *NeuroImage*, *160*, 41–54. https://doi.org/10.1016/j.neuroimage.2016.12.061

Purnell, B. S., Thijs, R. D., & Buchanan, G. F. (2018). Dead in the night: Sleep-wake and time-of-day influences on sudden unexpected death in epilepsy. *Frontiers in Neurology*, *9*, 5–8. https://doi.org/10.3389/fneur.2018.01079

Rai, S., Graff, K., Tansey, R., & Bray, S. (2024). How do tasks impact the reliability of fMRI functional connectivity? *Human Brain Mapping*, *45*(3), 1–20. https://doi.org/10.1002/hbm.26535

Rajpoot, K., Riaz, A., Majeed, W., & Rajpoot, N. (2015). Functional connectivity alterations in epilepsy from resting-state functional MRI. *PLoS One*, *10*(8), 3–5. https://doi.org/10.1371/journal.pone.0134944

Ruggiero, D. A., Mraovitch, S., Granata, A. R., Anwar, M., & Reis, D. J. (1987). A role of insular cortex in cardiovascular function. *Journal of Comparative Neurology*, *257*(2), 189–207. https://doi.org/10.1002/cne.902570206

Ryvlin, P., Nashef, L., Lhatoo, S. D., Bateman, L. M., Bird, J., Bleasel, A., Boon, P., Crespel, A., Dworetzky, B. A., Høgenhaven, H., Lerche, H., Maillard, L., Malter, M. P., Marchal, C., Murthy, J. M. K., Nitsche, M., Pataraia, E., Rabben, T., Rheims, S., … Tomson, T. (2013). Incidence and mechanisms of cardiorespiratory arrests in epilepsy monitoring units (MORTEMUS): A retrospective study. *The Lancet Neurology*, *12*(10), 966–977. https://doi.org/10.1016/S1474-4422(13)70214-X

Sainju, R. K., Dragon, D. N., Winnike, H. B., Nashelsky, M. B., Granner, M. A., Gehlbach, B. K., & Richerson, G. B. (2019). Ventilatory response to CO 2 in patients with epilepsy. *Epilepsia*, *60*(3), 508–517. https://doi.org/10.1111/epi.14660

Salek-Haddadi, A., Diehl, B., Hamandi, K., Merschhemke, M., Liston, A., Friston, K., Duncan, J. S., Fish, D. R., & Lemieux, L. (2006). Hemodynamic correlates of epileptiform discharges: An EEG-fMRI study of 63 patients with focal epilepsy. *Brain Research*, *1088*(1), 148–166. https://doi.org/10.1016/j.brainres.2006.02.098

Saper, C. B. (1982). Convergence of autonomic and limbic connections in the insular cortex of the rat. *Journal of Comparative Neurology*, *210*(2), 163–173. https://doi.org/10.1002/cne.902100207

Savva, A. D., Kassinopoulos, M., Smyrnis, N., Matsopoulos, G. K., & Mitsis, G. D. (2020). Effects of motion related outliers in dynamic functional connectivity using the sliding window method. *Journal of Neuroscience Methods*, *330*, 108519. https://doi.org/10.1016/j.jneumeth.2019.108519

Seeley, W. W., Menon, V., Schatzberg, A. F., Keller, J., Glover, G. H., Kenna, H., Reiss, A. L., & Greicius, M. D. (2007). Dissociable intrinsic connectivity networks for salience processing and executive control. *Journal of Neuroscience*, *27*(9), 2349–2356. https://doi.org/10.1523/JNEUROSCI.5587-06.2007

Sivathamboo, S., Friedman, D., Laze, J., Nightscales, R., Chen, MBiostat, Z., Kuhlmann, L., Devore, S., Macefield, V., Kwan, P., D'Souza, W., Berkovic, S. F., Perucca, P., O'Brien, T. J., & Devinsky, O. (2021). Association of short-term heart rate variability and sudden unexpected death in epilepsy. *Neurology*, *97*(24), e2357–e2367. https://doi.org/10.1212/wnl.0000000000012946

Song, X., Roy, B., Kang, D. W., Aysola, R. S., Macey, P. M., Woo, M. A., Yan-Go, F. L., Harper, R. M., & Kumar, R. (2018). Altered resting-state hippocampal and caudate functional networks in patients with obstructive sleep apnea. *Brain and Behavior*, *8*(6), 1–13. https://doi.org/10.1002/brb3.994

Sridharan, D., Levitin, D. J., & Menon, V. (2008). A critical role for the right fronto-insular cortex in switching between central-executive and default-mode networks. *Proceedings of the National Academy of Sciences of the United States of America*, *105*(34), 12569–12574. https://doi.org/10.1073/pnas.0800005105

Sveinsson, O., Andersson, T., Carlsson, S., & Tomson, T. (2017). The incidence of SUDEP: A nationwide population-based cohort study. *Neurology*, *89*(2), 170–177. https://doi.org/10.1212/WNL.0000000000004094

Sveinsson, O., Andersson, T., Mattsson, P., Carlsson, S., & Tomson, T. (2020). Clinical risk factors in SUDEP: A nationwide population-based case-control study. *Neurology*, *94*(4), e419–e429. https://doi.org/10.1212/WNL.0000000000008741

Szurhaj, W., Leclancher, A., Nica, A., Périn, B., Derambure, P., Convers, P., Mazzola, L., Godet, B., Faucanie, M., Picot, M. C., & De Jonckheere, J. (2021). Cardiac autonomic dysfunction and risk of sudden unexpected death in epilepsy. *Neurology*, *96*(21), e2619–e2626. https://doi.org/10.1212/WNL.0000000000011998

Tagliazucchi, E., & Laufs, H. (2014). Decoding wakefulness levels from typical fMRI resting-state data reveals reliable drifts between wakefulness and sleep. *Neuron*, *82*(3), 695–708. https://doi.org/10.1016/j.neuron.2014.03.020

Tang, Y., Chen, Q., Yu, X., Xia, W., Luo, C., Huang, X. Q., Tang, H., Gong, Q. Y., & Zhou, D. (2014). A resting-state functional connectivity study in patients at high risk for sudden unexpected death in epilepsy. *Epilepsy and Behavior*, *41*, 33–38. https://doi.org/10.1016/j.yebeh.2014.08.140

Thurman, D. J., Hesdorffer, D. C., & French, J. A. (2014). Sudden unexpected death in epilepsy: Assessing the public health burden. *Epilepsia*, *55*(10), 1479–1485. https://doi.org/10.1111/epi.12666

Thurman, D. J., Logroscino, G., Beghi, E., Hauser, W. A., Hesdorffer, D. C., Newton, C. R., Scorza, F. A., Sander, J. W., & Tomson, T. (2017). The burden of premature mortality of epilepsy in high-income countries: A systematic review from the Mortality Task Force of the International League Against Epilepsy. *Epilepsia*, *58*(1), 17–26. https://doi.org/10.1111/epi.13604

Uddin, L. Q., Kelly, A. M. C., Biswal, B. B., Castellanos, F. X., & Milham, M. P. (2009). Functional connectivity of default mode network components: Correlation, anticorrelation, and causality. *Human Brain Mapping*, *30*(2), 625–637. https://doi.org/10.1002/hbm.20531

Uddin, L. Q., Supekar, K., Lynch, C. J., Khouzam, A., Phillips, J., Feinstein, C., Ryali, S., & Menon, V. (2013). Salience network-based classification and prediction of symptom severity in children with autism. *JAMA Psychiatry*, *70*(8), 869–879. https://doi.org/10.1001/jamapsychiatry.2013.104

Valenza, G., Sclocco, R., Duggento, A., Passamonti, L., Napadow, V., Barbieri, R., & Toschi, N. (2019). The central autonomic network at rest: Uncovering functional MRI correlates of time-varying autonomic outflow. *NeuroImage*, *197*, 383–390. https://doi.org/10.1016/j.neuroimage.2019.04.075

Van Essen, D. C., Smith, S. M., Barch, D. M., Behrens, T. E. J., Yacoub, E., & Ugurbil, K. (2013). The WU-Minn Human Connectome Project: An overview. *NeuroImage*, *80*, 62–79. https://doi.org/10.1016/j.neuroimage.2013.05.041

Vilella, L., Lacuey, N., Hampson, J. P., Rani, M. R. S., Sainju, R. K., Friedman, D., Nei, M., Strohl, K., Scott, C., Gehlbach, B. K., Zonjy, B., Hupp, N. J., Zaremba, A., Shafiabadi, N., Zhao, X., Reick-Mitrisin, V., Schuele, S., Ogren, J., Harper, R. M., … Lhatoo, S. D. (2019). Postconvulsive central apnea as a biomarker for sudden unexpected death in epilepsy (SUDEP). *Neurology*, *92*(3), E171–E182. https://doi.org/10.1212/WNL.0000000000006785

Vilella, L., Miyake, C. Y., Chaitanya, G., & Hampson, J. P. (2024). Incidence and types of cardiac arrhythmias in the peri-ictal period in patients having a generalized convulsive seizure. *Neurology*, *103*(1), 1–11. https://doi.org/10.1212/WNL.0000000000209501

Wong, C. W., DeYoung, P. N., & Liu, T. T. (2016). Differences in the resting-state fMRI global signal amplitude between the eyes open and eyes closed states are related to changes in EEG vigilance. *NeuroImage*, *124*, 24–31. https://doi.org/10.1016/j.neuroimage.2015.08.053

Wong, C. W., Olafsson, V., Tal, O., & Liu, T. T. (2013). The amplitude of the resting-state fMRI global signal is related to EEG vigilance measures. *NeuroImage*, *83*, 983–990. https://doi.org/10.1016/j.neuroimage.2013.07.057

Wu, P., Bandettini, P. A., Harper, R. M., & Handwerker, D. A. (2015). Effects of thoracic pressure changes on MRI signals in the brain. *Journal of Cerebral Blood Flow and Metabolism*, *35*(6), 1024–1032. https://doi.org/10.1038/jcbfm.2015.20

Xifra-Porxas, A., Kassinopoulos, M., & Mitsis, G. D. (2021). Physiological and motion signatures in static and time-varying functional connectivity and their subject identifiability. *ELife*, *10*, e62324. https://doi.org/10.7554/eLife.62324

Yeo, T. B. T., Krienen, F. M., Sepulcre, J., Sabuncu, M. R., Lashkari, D., Hollinshead, M., Roffman, J. L., Smoller, J. W., Zöllei, L., Polimeni, J. R., Fischl, B., Liu, H., & Buckner, R. L. (2011). The organization of the human cerebral cortex estimated by intrinsic functional connectivity. *Journal of Neurophysiology*, *106*(3), 1125–1165. https://doi.org/10.1152/jn.00338.2011

Yoo, K., Rosenberg, M. D., Hsu, W. T., Zhang, S., Li, C. S. R., Scheinost, D., Constable, R. T., & Chun, M. M. (2018). Connectome-based predictive modeling of attention: Comparing different functional connectivity features and prediction methods across datasets. *NeuroImage*, *167*, 11–22. https://doi.org/10.1016/j.neuroimage.2017.11.010

Zaki, J., Ian, J., & Ochsner, K. N. (2012). Overlapping activity in anterior insula during interoception and emotional experience. *NeuroImage*, *62*(1), 493–499. https://doi.org/10.1016/j.neuroimage.2012.05.012

Zelano, C., Jiang, H., Zhou, G., Arora, N., Schuele, S., Rosenow, J., & Gottfried, J. A. (2016). Nasal respiration entrains human limbic oscillations and modulates cognitive function. *Journal of Neuroscience*, *36*(49), 12448–12467. https://doi.org/10.1523/JNEUROSCI.2586-16.2016